

Dimensional crossover of transport characteristics in topological insulator nanofilms

Koji Kobayashi¹, Ken-Ichiro Imura², Yukinori Yoshimura², and Tomi Ohtsuki¹

¹Department of Physics, Sophia University, Tokyo Chiyoda-ku 102-8554, Japan and

²Department of Quantum Matter, AdSM, Hiroshima University, Higashi-Hiroshima 739-8530, Japan

(Dated: December 7, 2024)

We show how the two-dimensional (2D) topological insulator evolves, by stacking, into a strong or weak topological insulator (STI or WTI) with different topological indices, proposing a new conjecture that goes beyond an intuitive picture on the quantum spin Hall (QSH) to the WTI crossover. Studying the conductance under different boundary conditions, we demonstrate the existence of two conduction regimes in which conduction happens either through the slab- or the edge-conduction channels, but not through both of them; the two conduction regimes are complementary and exclusive. Conductance maps are introduced, describing the dimensional crossover of the conductance from the 2D (single layer) to the 3D (infinite number of layers) limit. Stacking layers is an effective way of inverting the gap, alternative to controlling the strength of spin-orbit interaction. The emerging QSH phase is not restricted to the case of odd numbers of layers.

PACS numbers: 73.20.At, 73.61.-r 73.63.-b 73.90.+f

Three-dimensional (3D) topological insulators are classified into weak and strong [1–3], depending on the number of gapless (Dirac) points in the surface Brillouin zone. The strong topological insulator (STI) exhibits an odd number of Dirac cone that is robust against disorder [4–7]. The surface state of a weak topological insulator (WTI) with an even number of Dirac cones is superior in controllability, e.g., its transport characteristic is sensitive to nanoscale formations of the sample [8].

The existence of a topologically protected surface state of now a collection of STIs [9] has been repeatedly confirmed by spin-resolved ARPES measurements [10]. Recently, a WTI has been also experimentally identified [11]. Yet, as for triggering the topological nature in the transport characteristics, trials done for 3D bulk systems have been unsuccessful due to the difficulty of separating bulk and surface contributions to transport quantities [12]. In this sense, experimental observation of the topological nature in transport is yet restricted to 2D [13], and a natural step forward is to extend this 2D result to the case of 3D TI nanofilms [14–18]. Indeed, study of topological insulator nanofilms is of great interest recently not only in its original but also in related contexts [19–22].

There exists a simple picture on the construction of a WTI in which WTI is viewed as stacked layers of quantum spin Hall (QSH) states, *i.e.*, $(\text{QSH})^N \simeq \text{WTI}$ (where N is the number of stacked QSH layers) [21–26]. This is indeed a useful point of view, explaining how the helical edge state of a 2D QSH state evolves into the even number of Dirac cones on the surface of a WTI. Here, we highlight and examine how precisely the above point of view can be applied to the description of the actual crossover between the 2D and 3D limits in realistic slab-shaped samples (nanofilms) of a TI [27–33]. Conductance under different boundary conditions has been studied numerically (see Fig. 1).

Through this numerical study we show that the sim-

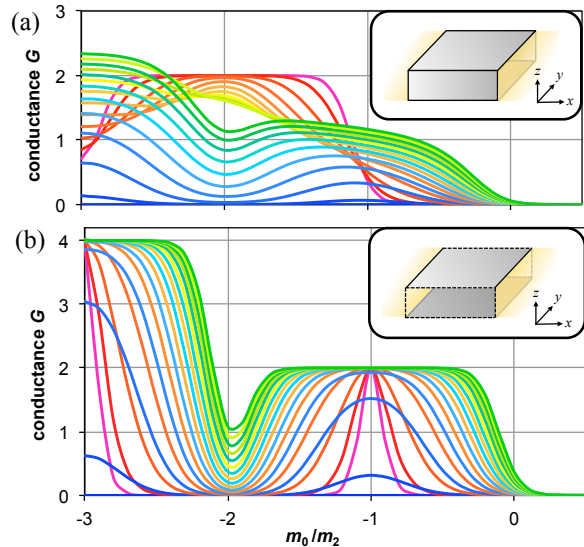


FIG. 1. (color online). Conductance of TI nanofilms. Different colors correspond to different layer numbers; warm (cold) colors correspond to odd (even) number of stacked layers. Boundary condition for the side surfaces: open in (a), periodic in (b).

ple $(\text{QSH})^N \simeq \text{WTI}$ picture does not literally work, or sometimes completely fails in the description of aforementioned crossover. The stacked layer of QSH does not necessarily evolve into a WTI state with specific weak indices $\nu = (\nu_1, \nu_2, \nu_3)$. In the intuitive picture the top and bottom surfaces [hereafter, chosen normal to the $(0, 0, 1)$ -direction] are always gapped and insulating; no Dirac cone on these surfaces, implying $\nu = (0, 0, 1)$ [8, 23–25]. In reality, the destined 3D bulk (topological) phase at the end of the stacking can be also an STI or a WTI phases with different topological indices. In a sense, this must be the case in that the phase diagram of a 3D TI is much more complex involving STI and WTI phases specified

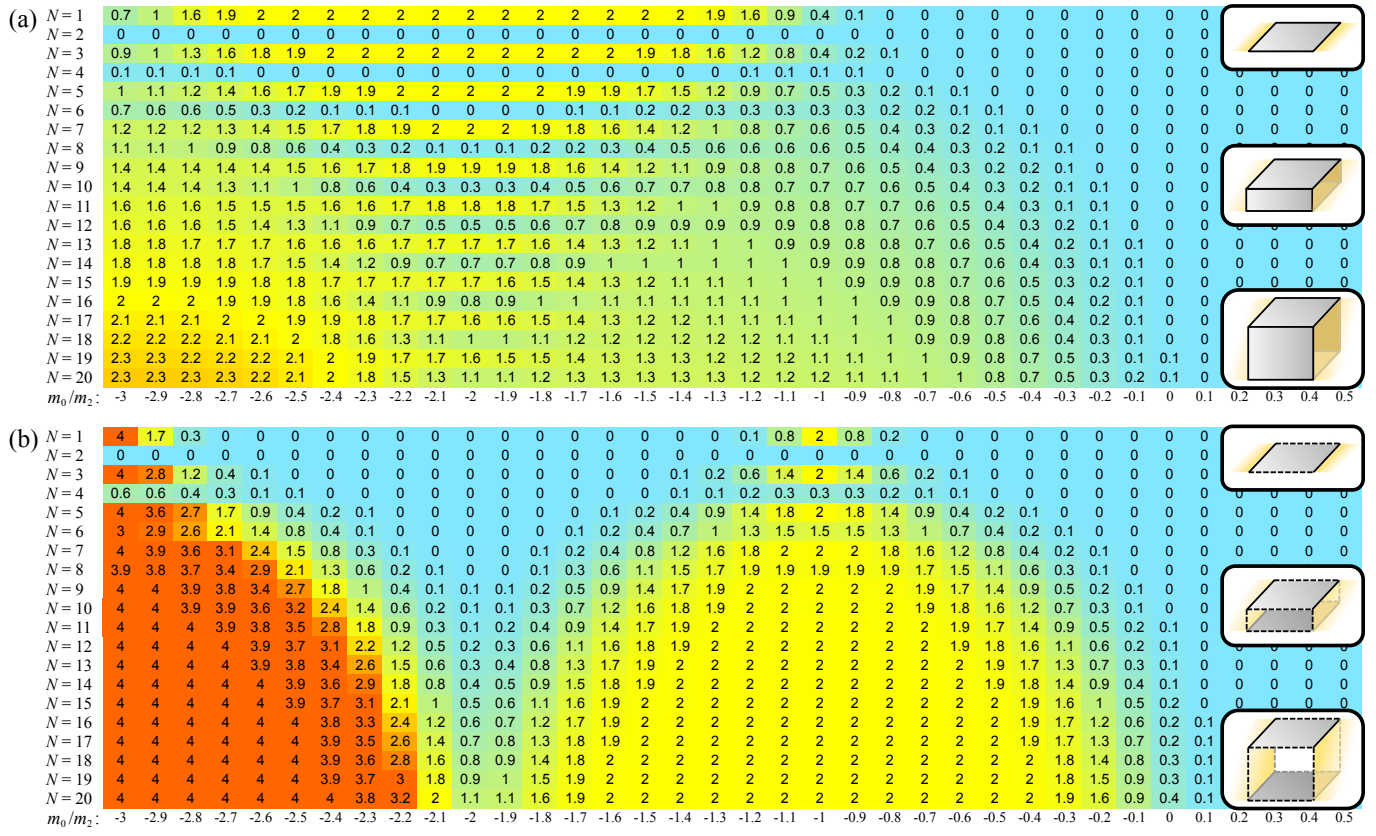


FIG. 2. (color online). Conductance maps for different [(a) open vs. (b) periodic] boundary conditions applied to a pair of side surfaces (y -sides), while the others (x -sides) are connected to ideal leads. The top/bottom surfaces (z -sides) are truncated. Calculated values of the conductance G (in units of e^2/h) at different values of the gap parameter m_0/m_2 and film thickness N are tabled and highlighted by a color scale. In (a) an alternate pattern of the conductance quantized either at $G = 2$ or at $G = 0$ characterizes the “edge-conduction” regime (yellow/blue striped region). In (b) “plateaus” of the conductance at $G = 2$ (and at $G = 4$) [yellow (red) regions] correspond to the “slab-conduction” regimes.

by four topological indices, ν_0 and ν , while its 2D counterpart is much simpler exhibiting only the quantum spin Hall and ordinary insulator (OI) phases distinguished by a single \mathbb{Z}_2 number, $\tilde{\nu}_0$ [34].

The second part of the “(QSH) $^N \simeq$ WTI” picture is on the even/odd feature, with respect to N . An even number N of edge modes circulating around the periphery of 3D TI nanofilms, stacked and hybridized tend to be gaped, while among an odd number of similar edge modes one remains gapless; the conductance map shown in Fig. 2(a) indeed confirms this even/odd feature. However, as demonstrated in Fig. 5, such a simple even/odd feature can be seen only in a limited range of parameter set. More generally, the global stripe pattern remains, while a new mechanism enters to achieve conductance plateaus at even number of layers.

Model— As a model for a 3D disordered TI, we consider the following Wilson-Dirac model, here implemented as a tight-binding Hamiltonian on a cubic lattice:

$$H(\mathbf{k}) = m(\mathbf{k})\tau_z + t \sin k_\mu \tau_x \sigma_\mu, \quad (1)$$

where $m(\mathbf{k}) = m_0 + m_{2\mu}(1 - \cos k_\mu)$, and the length unit

is set to the lattice constant. In the formulas repeated index μ ($= x, y, z$) is to be summed. Note also that $H(\mathbf{k})$ is a 4×4 matrix, spanned by two types of Pauli matrices σ and τ each representing physically real and orbital spins. The two terminal conductance G in units of e^2/h at Fermi energy $E = 0$ is obtained by the Landauer formula from the transmission coefficients calculated via the transfer matrix method [6].

Two panels of Fig. 1 show calculated conductance of the TI nanofilms. Different curves correspond to the films of different thickness, and describe evolution of the conductance as thickness is increased. The top and the bottom surfaces of the film is normal to the z -direction, while extremities on the x -axis is attached to the leads (see the inset of Fig. 1). The conductance plateaus in different boundary conditions [(a) open and (b) periodic] in y -direction highlight two different conduction regimes: (a) “edge-conduction” regime where the current flows on the y -sides of the sample, and (b) “slab-conduction” regime where the current flows on the top and bottom surfaces. To clarify the nature of these plateaus and of the evolution of the conductance as a function of the film thick-

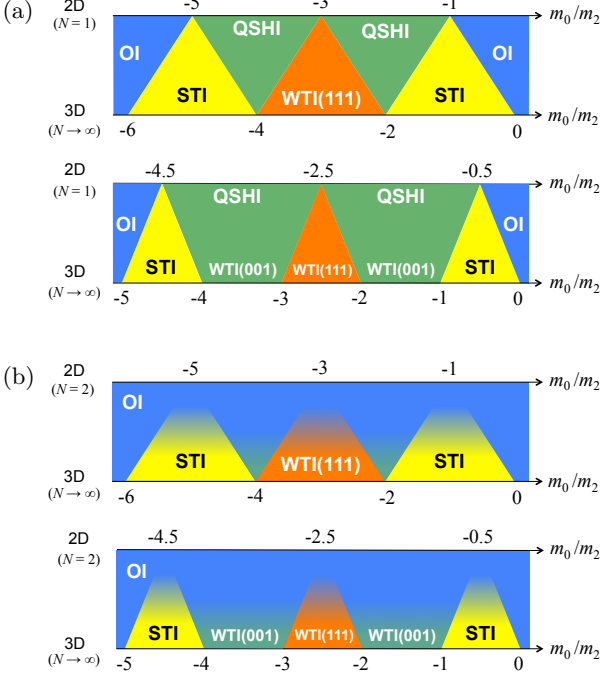


FIG. 3. (color online). Schematic phase diagram of the TI nanofilm. Cases of (a) N odd, (b) N even. In each panel, (upper) the isotropic system: $m_{2x} = m_{2y} = m_{2z} = m_2$, (lower) an anisotropic system: $m_{2x} = m_{2y} = m_2$, $m_{2z} = m_2/2$. The green areas [containing the QSHI and WTI(001) phases] represent the edge-conduction regimes, and the yellow (red) areas [containing the STI (isotropic WTI) phases and 2D phase boundaries] represent the slab-conduction regimes.

ness, we have replotted the same data in the form of a “conductance map” in Fig. 2. The two conductance maps, Fig. 2(a), (b), correspond to Fig. 1(a), (b), respectively.

Crossover from 2D to 3D— Let us look closely into evolution of the conductance between 2D and 3D limits. We first focus on behaviors on the isotropic system: $m_{2\mu} = m_2$ ($\mu = x, y, z$), and set the parameter $t/m_2 = 2$. Fig. 2(a) shows evolution of the conductance with open boundary conditions on the y -side as the thickness is increased. We have studied this evolution at different model parameters m_0/m_2 , *i.e.*, in cases of the different starting 2D systems, either being a QSH or an OI. The size of the system is such that the top and bottom surfaces are of size $L_x \times L_y = 20 \times 20$, while the thickness N of the film is varied from 1 to 20.

In Fig. 2(a) an upside-down triangle area shows stripes of conductance plateaus, where the conductance is almost quantized at $G = 2$ ($G = 0$) for relatively small odd (even) number of layers N . At $N = 1$, the system is a QSH insulator: $\tilde{\nu}_0 = 1$ in the range of $-3 < m_0/m_2 < -1$, while $\tilde{\nu}_0 = 0$ when $-1 < m_0/m_2$. Stacking such layers in the z -direction one can compose a TI nanofilm with surface states circulating around the side surfaces leaving the top and the bottom surfaces gapped. As long as N

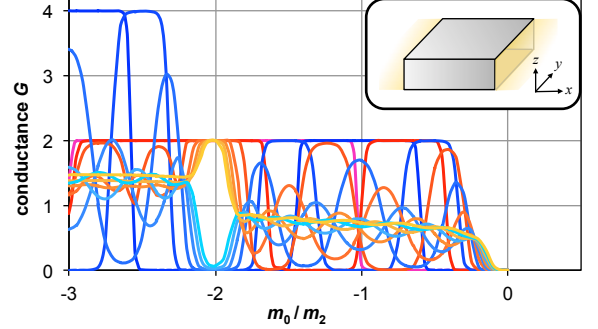


FIG. 4. (color online). Conductance of TI nanofilms as in Fig. 1(a) but with $t/m_2 = 0.5$. In contrast to Fig. 1(a), the behavior of the conductance looks rather erratic.

is *odd*, the side surfaces remain gapless and the conductance shows a plateau at $G = 2$ implying the existence of a pair of perfectly conducting channels, while practically vanishing conductances are observed at N even. This seems, at first, consistent with the simple “ $(QSH)^N \simeq \text{WTI}$ ” picture. However, the simple picture does not imply that this region showing the expected even/odd feature shrinks as the thickness N is increased. Nor does it imply that in the limit of $N \rightarrow \infty$ there is no expected WTI state with weak indices $\nu = (0, 0, 1)$. In the 3D limit, $N \rightarrow \infty$, the system is in the trivial insulator phase if $0 < m_0/m_2$, in the STI phase if $-2 < m_0/m_2 < 0$, and in the WTI phase with weak indices $\nu = (1, 1, 1)$ if $-4 < m_0/m_2 < -2$. The phase diagram of the system is symmetric with respect to $m_0/m_2 = -3$.

As the even/odd feature is washed out with increasing N , quantized conductance appears as a new emergent feature in the two triangular regions, pointing upwards, adjacent to the upside-down striped triangle [see Fig. 2(b)]. The quantized conductance on the stripes of the upside-down triangle area in panel (a) was due to the edge modes circulating around the side surfaces, and in this sense this area can be regarded as the “edge-conduction” regime. In the periodic boundary on the y -sides the edge-conduction does not contribute to the conductance. As a result, the stripe pattern in the upside-down triangle disappear in panel (b); the conductance becomes practically vanishing. On the contrary, in the adjacent triangles the conductance tends to be quantized either at $G = 2$ or at $G = 4$, depending on whether the destination in the $N \rightarrow \infty$ limit is an STI or a WTI. These quantizations are due to contributions from Dirac cones at the top and the bottom surfaces [6], and in this sense the two triangular area can be regarded as the “slab-conduction” regime.

In Fig. 3 we first divided the conductance map into cases of odd and even number of layers, then abstracted it into the form of a schematic phase diagram. The upper panels of (a) and (b) correspond to the case of odd and even number of layers for the isotropic case:

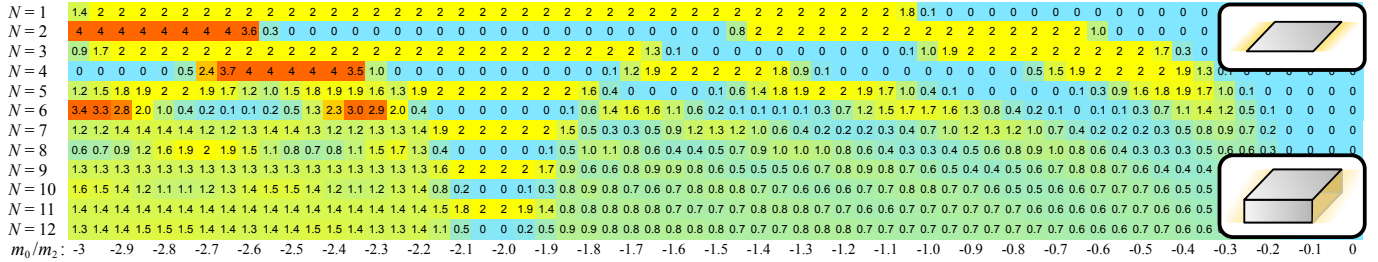


FIG. 5. (color online). Conductance map with $t/m_2 = 0.5$. New valleys and plateaus emerge, while simple even/odd feature as in Figs. 2 and 3 breaks down.

$m_{2x} = m_{2y} = m_{2z} = m_2$, while the lower panels describe an anisotropic case: $m_{2x} = m_{2y} = m_2$, $m_{2z} = m_2/2$. In this anisotropic system there exists indeed a range of parameters $-2 < m_0/m_2 < -1$ in which “(QSH) N ” leads to an expected WTI with $\nu = (0, 0, 1)$ state [35].

Complementarity and exclusiveness of the edge and the slab-conduction regimes— As we have seen so far, conduction in the TI nanofilm is caused either by the slab-, or by the edge-conducting channel. The two types of conducting channels do not become completely open at the same time, while either of the channels is open except in the crossover regime at which both of the channels are partially open.

An alternative view from the 3D limit— In the 3D limit on the bottom line of Fig. 2 (b) the STI phase is extended over $-2 < m_0/m_2 < 0$. In STIs gapless surface states appear on all surfaces available: the top and bottom of the slab-shaped sample. Penetration of such a surface state becomes deeper as one approaches the phase boundary at $m_0/m_2 = 0, -2$ (where the Dirac semimetal phase appears). There, as one reduces the number of layers N , a hybridization gap is formed more easily, driving the system to the edge-conduction regime at relatively large N . Quantization of the conductance in the slab-conduction region is due to Dirac cones at the top and the bottom surfaces [6]. With decreasing N such perfect conduction is naturally destroyed, while at the center of the STI phase at $m_0/m_2 = -1$ the slab-conduction survives exceptionally down to the single-layer (2D) limit: $N = 1$. At this value of m_0/m_2 the surface wave function is oscillatory and vanishes at odd numbers' layer. As a result, the hybridization gap does not open as far as N is odd.

Breakdown of the even/odd feature— Figure 4 shows evolution of the conductance in an isotropic system at $t/m_2 = 0.5$ varying the film thickness under the open boundary condition as in Fig. 1(a). The behavior of the conductance in Fig. 4 looks much irregular compared with Fig. 1(a). Figure 5 shows a conductance map corresponding to Fig. 4. In the upside-down triangular region around $m_0/m_2 = -2$, one can observe that the evolution of the even/odd stripe pattern as in Fig. 2(a) remains. In contrast to Fig. 2(a), new plateaus are observed outside the upside-down triangular region, and even in the

even number of layers. The breakdown of the even/odd feature occurs in the parameter regimes at which penetration of the surface state into the bulk is oscillatory, inducing “inversion” of the hybridization gap.

In Fig. 5 at $N = 2$ the conductance is *a priori* supposed to vanish (“valley” of the conductance), while in the range of $-1.4 \lesssim m_0/m_2 \lesssim -0.65$, it jumps to a quantized value $G = 2$. Similarly, on the other side, around $m_0/m_2 \lesssim -2.6$ it is again quantized at $G = 4$. The border between the original conductance valley and the new plateau is roughly located at the vanishing of the renormalized mass, $\tilde{m}_{0,N=2} = m_0 + m_2 \pm m_2/2$. On the contrary, at $N = 3$ the conductance is *a priori* quantized at $G = 2$, while this original plateau is replaced by a new valley around $-1.6 \lesssim m_0/m_2$, then reappears, forming a new plateau in the range: $-0.95 \lesssim m_0/m_2 \lesssim -0.45$. The borders between the two plateaus and the new valley are again given by the vanishing of $\tilde{m}_{0,N=3} = m_0 + m_2 + \Delta m$, where $\Delta m = 0, \pm m_2/\sqrt{2}$. In the formulas for the renormalized mass $\tilde{m}_{0,N=2}$ and $\tilde{m}_{0,N=3}$, the last term arises due to the interlayer hopping of the form: $-m_2 \cos k_z \tau_z$ in Eq. (1). The new valleys and plateaus look as if they are extension of the even/odd stripes in the upside-down triangle area deformed at the periphery and outside of the original region.

What are the origins of these new valleys and plateaus? The *original* valley of the conductance that appears at an even number of layers in the upside-down triangle area is a consequence of the gapped spectrum; the size of the gap is determined by overlap of the top and bottom surface wave functions, *i.e.* by the remaining amplitude $\psi_{z=N}$ of the top surface wave function, initially with an amplitude $\psi_{z=1}$ at the opposing bottom surface. Here, in the present parameter regime the surface wave function is oscillatory, while the precise behavior of the damped oscillation varies as a function of model parameters. Thus, as changing the mass parameter m_0/m_2 , it happens that $\psi_{z=N}$ vanishes at a critical value of m_0/m_2 , then changes sign; correspondingly, the hybridization gap vanishes, then get “inverted”. In the regime of this inverted hybridization gap, there appear edge states just as in the usual QSH insulator phase.

To summarize, a simple picture of WTI based on

the observation: “(QSH) $^N \simeq$ WTI” has been questioned from two respects. First, stacking QSH insulators, *i.e.*, “(QSH) N ” does not lead necessarily to the expected WTI (0,0,1) state, but to a WTI with other indices or even to an STI as well. Secondly, since the hybridization gap can get *inverted* due to damped oscillation of the surface wave function, a simple even/odd feature with respect to the number of stacked layers fails. Our new conjecture on the two conduction regimes serves as a guideline to interpolate 2D and 3D limits. In this paper, the calculation has been performed in the absence of disorder for $E = 0$. We have checked our results are stable against disorder unless the bulk band gap closes [6, 7]. They are also robust against change of E as long as E is inside the bulk gap. Here, we assumed square film geometry ($L_x = L_y$). In the case of rectangular film ($L_x \gg L_y$), perfect conduction will be easier to observe. We finally mention that a phase diagram similar to Fig. 2, consisting of cross-dimensional topological regions has been proposed recently in an independent context, namely in that of cold atoms [20].

This work was supported by Grants-in-Aid for Scientific Research (C) (Grant No. 23540376) and Grants-in-Aid No. 24000013. K. I. acknowledges Y. Ando and Y. Takane for useful discussions.

[1] J. E. Moore and L. Balents, Phys. Rev. B **75**, 121306 (2007).
[2] L. Fu, C. L. Kane, and E. J. Mele, Phys. Rev. Lett. **98**, 106803 (2007).
[3] R. Roy, Phys. Rev. B **79**, 195322 (2009).
[4] R. Shindou and S. Murakami, Phys. Rev. B **79**, 045321 (2009).
[5] P. Goswami and S. Chakravarty, Phys. Rev. Lett. **107**, 196803 (2011).
[6] K. Kobayashi, T. Ohtsuki, and K.-I. Imura, Phys. Rev. Lett. **110**, 236803 (2013).
[7] K. Kobayashi, T. Ohtsuki, K.-I. Imura, and I. F. Herbut, Phys. Rev. Lett. **112**, 016402 (2014).
[8] Y. Yoshimura, A. Matsumoto, Y. Takane, and K.-I. Imura, Phys. Rev. B **88**, 045408 (2013).
[9] Y. Ando, Journal of the Physical Society of Japan **82**, 102001 (2013).
[10] M. Z. Hasan and C. L. Kane, Rev. Mod. Phys. **82**, 3045 (2010).
[11] B. Rasche, A. Isaeva, M. Ruck, S. Borisenko, V. Zabolotnyy, B. Büchner, K. Koepernik, C. Ortix, M. Richter, and J. van den Brink, Nature materials **12**, 422 (2013).
[12] S. Matsuo, K. Chida, D. Chiba, T. Ono, K. Slevin, K. Kobayashi, T. Ohtsuki, C.-Z. Chang, K. He, X.-C. Ma, et al., Phys. Rev. B **88**, 155438 (2013).
[13] M. König, S. Wiedmann, C. Brüne, A. Roth, H. Buhmann, L. W. Molenkamp, X.-L. Qi, and S.-C. Zhang, Science **318**, 766 (2007).
[14] Y. Zhang, K. He, C.-Z. Chang, C.-L. Song, L.-L. Wang, X. Chen, J.-F. Jia, Z. Fang, X. Dai, W.-Y. Shan, et al., Nature Physics **6**, 584 (2010).
[15] A. A. Taskin, S. Sasaki, K. Segawa, and Y. Ando, Phys. Rev. Lett. **109**, 066803 (2012).
[16] A. A. Taskin, S. Sasaki, K. Segawa, and Y. Ando, Advanced Materials **24**, 5581 (2012), ISSN 1521-4095.
[17] A. A. Taskin, F. Yang, S. Sasaki, K. Segawa, and Y. Ando, Phys. Rev. B **89**, 121302 (2014).
[18] C. Brüne, C. X. Liu, E. G. Novik, E. M. Hankiewicz, H. Buhmann, Y. L. Chen, X. L. Qi, Z. X. Shen, S. C. Zhang, and L. W. Molenkamp, Phys. Rev. Lett. **106**, 126803 (2011).
[19] X. Qian, L. Fu, and J. Li, arXiv:1403.3952 (2014).
[20] M. S. Scheurer, S. Rachel, and P. P. Orth, arXiv:1406.7396 (2014).
[21] H. Ozawa, A. Yamakage, M. Sato, and Y. Tanaka, Phys. Rev. B **90**, 045309 (2014).
[22] Y. Takane, J. Phys. Soc. Jpn. **83**, 103706 (2014).
[23] J. C. Y. Teo and C. L. Kane, Phys. Rev. B **82**, 115120 (2010).
[24] Z. Ringel, Y. E. Kraus, and A. Stern, Phys. Rev. B **86**, 045102 (2012).
[25] K.-I. Imura, M. Okamoto, Y. Yoshimura, Y. Takane, and T. Ohtsuki, Phys. Rev. B **86**, 245436 (2012).
[26] H. Obuse, S. Ryu, A. Furusaki, and C. Mudry, Phys. Rev. B **89**, 155315 (2014).
[27] J. Linder, T. Yokoyama, and A. Sudbø, Phys. Rev. B **80**, 205401 (2009).
[28] C.-X. Liu, H.-J. Zhang, B. Yan, X.-L. Qi, T. Frauenheim, X. Dai, Z. Fang, and S.-C. Zhang, Phys. Rev. B **81**, 041307 (2010).
[29] H.-Z. Lu, W.-Y. Shan, W. Yao, Q. Niu, and S.-Q. Shen, Phys. Rev. B **81**, 115407 (2010).
[30] W.-Y. Shan, H.-Z. Lu, and S.-Q. Shen, New Journal of Physics **12**, 043048 (2010).
[31] K. Ebihara, K. Yada, A. Yamakage, and Y. Tanaka, Physica E: Low-dimensional Systems and Nanostructures **44**, 885 (2012).
[32] M. Okamoto, Y. Takane, and K.-I. Imura, Phys. Rev. B **89**, 125425 (2014).
[33] J. Zhou, W. Feng, G. Liu, and Y. Yao, arXiv:1409.0943 (2014).
[34] C. L. Kane and E. J. Mele, Phys. Rev. Lett. **95**, 146802 (2005).
[35] The isotropic case discussed earlier was slightly exceptional; the WTI phase with weak indices $\nu = (0, 0, 1)$ becomes extinct.